Chemical Engineering Research and Design 220 (2025) 49–58

Contents lists available at ScienceDirect

Chemical Engineering Research and Design

journal homepage: www.elsevier.com/locate/cherd

Theoretical adsorption modeling and simulation of toxic arsenic ions removal in batch and continuous systems using Mn/Mg/Fe layered double hydroxides

Nguyen Thi Hai [a,b], Seongchul Ryu [c], Paripurnanda Loganathan [d], Jaya Kandasamy [d], Saravanamuthu Vigneswaran [d], Tien Vinh Nguyen [d,*]

[a] VNU Key Laboratory of Geoenvironment and Climate Change Response, University of Science, Vietnam National University, Hanoi, Viet Nam
[b] University of Science, Vietnam National University, Hanoi, Viet Nam
[c] Osmoflo, South Australia, Australia
[d] Faculty of Engineering and IT, University of Technology Sydney (UTS), Sydney, Australia

ARTICLE INFO

Keywords:
Arsenic removal
Adsorption
Layered double hydroxides
Pore diffusion model
Simulation
Water treatment

ABSTRACT

Groundwater contaminated by arsenic (As) presents an increasingly important challenge in many countries throughout the world because of the danger it poses to the health of humans, flora and fauna. The main challenge in research on removing As from groundwater is the need to test under several experimental conditions to optimise the parameters for adsorption column studies. This study aims to develop a robust mathematical model that enhances the operational conditions of dynamic adsorption columns based on limited laboratory experimental data. In this study, after batch experiments, two columns experiment with a synthesized layered double hydroxide (Mn/Mg/Fe-LDH) adsorbent were applied to investigate the adsorbent's performance in removing As ions, specifically As(III) and As(V), from synthetic water. Using the same experimental conditions (filtration rate 0.75 m/h, bed height 0.09 m, and inlet As concentration 0.33 mg/L), the exhaustion time for Mn/Mg/Fe-LDH in the removal of As(III) amounted to 280 days, which was longer than 180 days for As(V). The dynamic adsorption column model, which utilized the pore diffusion model (PDM) in conjunction with the Sips equation parameters, effectively simulated the breakthrough curves from the column experiments. The breakthrough curves were successfully simulated for a range of adsorption conditions such as bed height of 0.045–0.135 m, filtration rate of 0.75–1.25 m/h, and initial As(V) concentration of 0.033–3.333 mg/L. Characterization of the Mn/Mg/Fe-LDH adsorbent before and after the adsorption process indicated that the main mechanisms for As(III) and As(V) removal included oxidation-couples adsorption and reduction-coupled oxidation, respectively.

1. Introduction

Arsenic (As) is recognized as a significant groundwater contaminant worldwide. Its occurrence in water bodies is attributed to both natural processes and human activities including geological weathering and volcanic activity, industrial practices (mining and non-ferrous metal smelting), and agricultural activities (developing and using pesticides, herbicides, insecticides) (Kim et al., 2012; Smedley and Kinniburgh, 2002). According to reports by (Siddiqui and Chaudhry, 2017), in natural water bodies, two inorganic species of As (As(V) and As(III)) have been reported as the most common toxic form. As(III) is considerably more dangerous and mobile than As(V) (Smedley and Kinniburgh, 2002). The health risks associated with long-term contact with As-contaminated water are severe and well-documented. Prolonged consumption of such water can lead to numerous health problems, including skin diseases, tissue damage, and a heightened risk of various cancers (Jain and Chandramani, 2018). There is consequently a pressing need to effectively remove As from contaminated groundwater to ensure that communities have safe drinking water.

Several advanced and conventional treatment methods have been started and utilized to effectively remove As from aqueous environments (Singh et al., 2021; Weerasundara et al., 2021). The key technologies include adsorption, oxidation, phytoremediation, coagulation-flocculation, membrane filtration and ion exchange. Of these

* Corresponding author.
E-mail address: Tien.Nguyen@uts.edu.au (T.V. Nguyen).

https://doi.org/10.1016/j.cherd.2025.06.027
Received 9 January 2025; Received in revised form 18 June 2025; Accepted 18 June 2025
Available online 21 June 2025
0263-8762/© 2025 The Authors. Published by Elsevier Ltd on behalf of Institution of Chemical Engineers. This is an open access article under the CC BY license (http://creativecommons.org/licenses/by/4.0/).

technologies, adsorption is frequently considered the most effective option for decentralized water treatment systems because of its simplicity, inexpensiveness, straightforward design, ease of operation, and low waste production and maintenance requirements (Nguyen et al., 2020). Until now, various adsorbents have been explored for their capacity to adsorb As from aqueous solutions (Lata and Samadder, 2016; Nguyen et al., 2020; Pena et al., 2005). Among the publicly known adsorbents, layer double hydroxides (LDHs), referred to as a hydrotalcite-like adsorbent or synthesized clay, have proven to be particularly effective in removing As from the aqueous environment (Asiabi et al., 2017; Tran et al., 2019; Wang et al., 2018).

One of the LDHs's properties is the different ionic layers it contains and these help this adsorbent to exhibit high and versatile adsorption capacity. They include the brucite-like layers with a positive charge and the interlayer region containing anions with a negative charge, suggesting that it can effectively remove both cationic and anionic ions. Our previous study noted that a novel layered double hydroxide, designated as Mn/Mg/Fe-LDH, was created by the simple co-precipitation method derived from three inorganic salts: magnesium nitrate ($Mg(NO_3)_2$), manganese nitrate ($Mn(NO_3)_2$), and iron nitrate ($Fe(NO_3)_3$) (Nguyen et al., 2022). The synthesized Mn/Mg/Fe-LDH demonstrated a highly effective capacity for adsorbing both As(III) and As(V) ions (Nguyen et al., 2022). The Langmuir maximum adsorption capacity (Qmax) of Mn/Mg/Fe-LDH conducted at pH 7.0 and 25°C to As ions (As(III) at 56.1 mg/g; As(V) at 32.2 mg/g), was noticeably greater than the values of other adsorbents documented in the literature (Kalaruban et al., 2019; Lin et al., 2017; Nguyen et al., 2020; Nguyen et al., 2020).

Investigating the performance of Mn/Mg/Fe-LDH in fixed-bed column adsorption of As ions is very important because such experiments are conducted under dynamic conditions and generate useful information for practical applications. Examples here are the behavior of breakthrough curves and treatment performance statistics, which are critical for system design for the purpose of real-world applications. Thus, in this study, after batch experiments, two columns packed with Mn/Mg/Fe-LDH materials were employed to adsorb both As species [As (V) and As(III)] from synthetic water under dynamic conditions. Adsorption column experiments need to be executed under various operational scenarios to establish what are the best operational parameters for desired performance. This means in effect, utilizing more time at great expense.

Simulating As removal through theoretical adsorption modelling to evaluate and optimize the expected performance of Mn/Mg/Fe-LDH in both batch and column adsorption tests is considered a useful and cost-effective approach. This is because theoretical modelling helps researchers reduce the number of experiments that need to be run to adequately provide the model with the information required to identify the optimum conditions for a column adsorption test. Moreover, models can help researchers develop significant improvements in design for practical applications to be more cost-effective. In fact, a wide range of adsorption models have been developed to describe the behavior of adsorbents during the As adsorption process. Among these, the Langmuir, Freundlich, pseudo-first-order and pseudo-second-order, and Thomas, Bohart–Adams, and Yoon–Nelson models are commonly used for analyzing adsorption equilibrium, predicting adsorption rates and mechanisms, and for analyzing the adsorbent's behavior in fixed-bed adsorption systems, respectively (Asiabi et al., 2017; Luengo et al., 2023; Nguyen et al., 2022; Samsuri et al., 2013; Vancea et al., 2023). Vancea et al. (2023) used these models to determine the adsorption behavior and mechanism of unconventional material with iron content in removing As. However, the conventional kinetic models like the pseudo-first-order and pseudo-second-order help describe adsorption rates. Nonetheless they often oversimplify real systems by ignoring simultaneous processes such as film diffusion or surface reactions. Similarly, fixed-bed models like Thomas, Bohart–Adams, and Yoon–Nelson are easy to apply but rely on ideal assumptions, making them less accurate under varying conditions (initial concentration, flow rate, and bed height of column).

In contrast, the pore diffusion model (PDM) offers greater flexibility, as parameters like film mass transfer and pore diffusion coefficients - once determined – can serve to predict system performance under different concentrations and flow rates, reducing the need for repeated experiments. Despite the potential benefits of PDM models, it is worth noting that only a few studies applied the PDM model to determine and predict the performance of LDHs adsorbents for As removal under dynamic conditions (Lu et al., 2015). Moreover, there is a significant lack of studies that employ this mathematical model for analyzing the breakthrough curves of an adsorbent and the adsorbent's behavior in removing of both As(III) and As(V) in column adsorption tests. In light of this discrepancy, the present study seeks to apply a mathematical model, namely PDM, that simulates As removal from aqueous environments using Mn/Mg/Fe-LDH calibrated with results from a limited number of laboratory experiments.

2. Materials and methods

2.1. Materials and chemicals

Mn/Mg/Fe-LDH was prepared via the co-precipitation method using a metal molar ratio of 1:1:1. A solution containing 0.04 mol of Mn $(NO_3)_2$, $Mg(NO_3)_2{\bullet}6H_2O$ and $Fe(NO_3)_3{\bullet}9H_2O$ in 60 mL was added dropwise to another 60 mL solution consisting of 0.022 mol of Na_2CO_3 and 0.336 mol of NaOH and subjected to continuous stirring (Nguyen et al., 2022). The mixture was subsequently aged at a controlled temperature of 45°C for 3 h while maintaining pH 12 ± 0.2 so that the required precipitates could be obtained. The precipitated powder was filtered to isolate it from the mixture solution and thoroughly washed with DI-water when the pH of filtrated solution approached 7.0. Following this, the resultant substance was dried in an oven for 48 h at 80 °C before being transferred to an airtight container for storage.

2.2. Adsorption experiments

2.2.1. Equilibrium study

Adsorption isotherm analyses were conducted with initial As(V) and As(III) concentrations of 0–270 mg/L maintaining an initial pH of 7 ± 0.2, a temperature of 25 °C and adsorbent dosage of 0.5 g/L. These experiments were performed in triplicate, and the mean values with standard deviations are reported in Figs. 1 and 2. After 24 h shaking, the equilibrium adsorption capacity of Mn/Mg/Fe-LDH, can be computed as follows:

$$Q_e = \frac{V(C_i - C_e)}{m} \tag{1}$$

where: Q_e represents the amount of As adsorbed onto adsorbent (mg/g); m represents the mass of used adsorbent (g); C_i and C_e represent As(V) and As(III) concentrations at initial and equilibrium conditions (mg/L), respectively; and V represents the total volume of As(V) or As(III) solutions (L). Sips adsorption isotherm equation served to characterize the adsorption process (Kim et al., 2015) and is written as follows:

$$\text{Sips equation}: Q_e = \frac{Q_m b C_e^{1/n}}{(1 + b C_e^{1/n})} \tag{2}$$

where, Q_e represents the Mn/Mg/Fe-LDH capacity to adsorb As at equilibrium conditions (mg/g) and Q_m represents the Sips maximum removal capacity (mg/g). In the Sips isotherm model, the parameter b is a constant (L/mg) that reflects the binding sites' affinity, while the parameter dimension-less $1/n$ refers to the surface heterogeneity.

2.2.2. Kinetic study

Kinetic batch experiments were undertaken at various time intervals in the 1–1440 mins range, using initial concentrations of As(V)

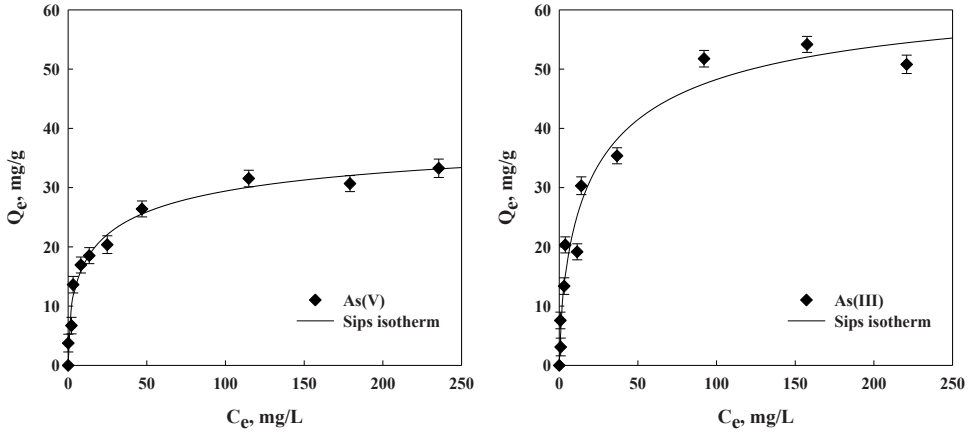

Fig. 1. Adsorption isotherm modeling for As(V) and As(III) adsorption onto Mn/Mg/Fe-LDH.

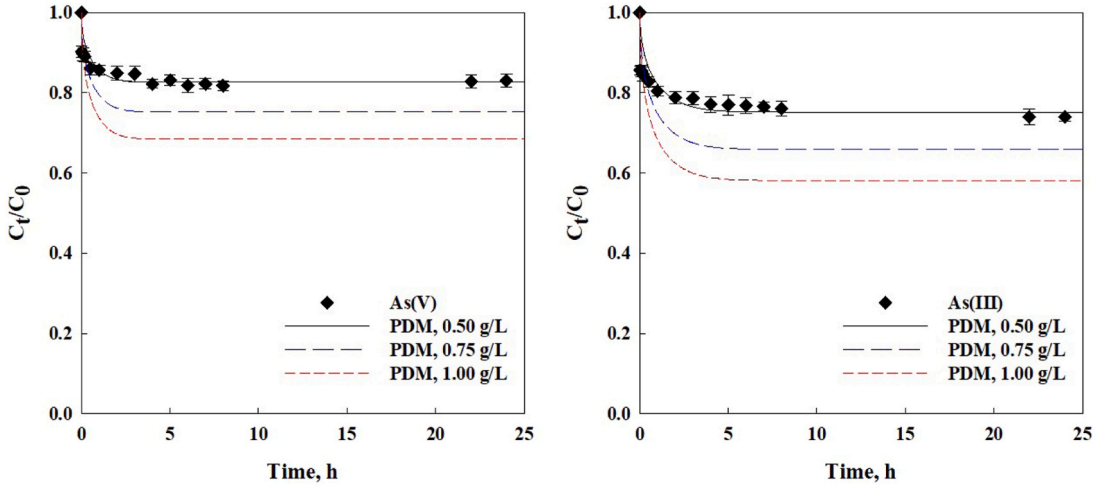

Fig. 2. Kinetic adsorption and prediction curves by PDM on Mn/Mg/Fe-LDH.

(74.35 mg/L) and As(III) (70.47 mg/L). The experiments were undertaken at room temperature and at pH = 7 ± 0.2 and a solid-to-liquid ratio of 0.5 g/L was used. Similarly, with the equilibrium adsorption, experiments were conducted in triplicate, and the results were shown as mean values with error bars. Kinetic adsorption parameters were examined using the pore diffusion model (PDM). The absorbate mass transfer equations used in PDM are described below and they are based on the subsequent presumptions (Ponnusami et al., 2010):

i) The adsorbent particle is globular.
ii) The work solution is diluted and in local equilibrium state.
iii) The adsorption operates isothermally.

$$\varepsilon_p \frac{\partial C_p}{\partial t} + \rho_p \frac{\partial Q}{\partial t} = \frac{\varepsilon_p}{r^2} \frac{\partial}{\partial r}\left(r^2 D_p \frac{\partial C_p}{\partial r}\right) \quad (3)$$

$$k_f (C - C_s) = \varepsilon_p D_p \frac{\partial C_p}{\partial r} atr = R_p \quad (4)$$

$$\frac{\partial C_p}{\partial r} = 0 atr = 0 \quad (5)$$

$$C_p = C_{p0}, \quad q = q_0 att = 0 \quad (6)$$

While the pore diffusion model (PDM) was selected for its suitability in capturing intraparticle diffusion mechanisms, the comparative modeling with alternative approaches (e.g., LDFA or surface diffusion models) may offer additional insights. Future studies will explore such comparisons to further validate and refine the model's robustness.

2.3. Characterization of adsorbent

The scanning electron microscope (SEM) integrated with energy-dispersive X-ray spectroscopy (EDS) helped to establish the adsorbent's morphology and main elements using Quanta-650 machine. The X-ray Diffractometer (XRD) and Fourier transform infrared spectrometer (FTIR) were employed to detect the adsorbent's crystalline structure and primary functional groups existing on the external surface of adsorbents, using Rigaku MiniFlex 600 and Jasco-4600 machines, respectively.

2.4. Column study

Column adsorption studies employed four glass columns with a total height of 0.11 m and an inner radius of 4.5 mm. These columns were tested to evaluate the adsorption behavior of both As ions under controlled and consistent experimental conditions. Master flex L/S at a steady 0.75 m/h filtration rate pumped the 0.33 mg/L feed solution in upward flow modus through a vertical column. The bed-column was filled with 5 g of Mn/Mg/Fe LDH which achieved a bed height of 0.09 m. The acrylic beads and cotton balls of 1.0 mm were then positioned at the bottom and top of the column to retain the packed adsorbent intact.

The column adsorption experiments were carried out over an extensive period lasting 320 days. Effluent samples were taken for

weekly monitoring until the As concentration returned to the initial level. Then - using 0.45 μm filters - the samples were filtered, and the resulting effluents were examined for As via an inductively coupled plasma mass spectrometry (ICPMS-NexION 2000, US).

Three models, namely Bohart-Adams, Thomas and Yoon-Nelson, can describe adsorption behavior in the fixed-bed system and their simplicity explains their widespread usage (Brion-Roby et al., 2018; Chu, 2020). Despite the fact that they fit well with breakthrough curves observed in a column, when it runs out from the asymptotic limit, what becomes more important is the mass transfer control and axial dispersion. Much effort is required to calibrate the model parameters for dynamic models, for instance the mass transfer model and dispersed plug flow model (Inglezakis et al., 2018). According to Cruz-Olivares et al. (2013), for this reason, it is appropriate to simulate a fixed-bed experiment loaded with Mn/Mg/Fe-LDH when assuming the following:

i) The column system operates under isothermal conditions.
ii) The Mn/Mg/Fe-LDH adsorbent is sphere-shaped and homogeneously filled in the column.
iii) The adsorbent is characterized by homogenous pore size distribution and having a uniform pore structure.
iv) Radial concentration gradients are considered negligible.
v) The physical characteristics of fluid utilized in the fixed-bed column are constant.
vi) The flow pattern is a distributed plug flow moving at a steady linear pace.
vii) The gradient of the concentration inside the particle echoes the parabolic shape.

PDM is the column model employed and it originates from the energy equation and mass balance. A two-dimensional PDM model can estimate the spread of the breakthrough curve. The model is referred to as two-dimensional due to its treatment of both axial transport in the packed bed and radial diffusion within the adsorbent particles, consistent with intraparticle mass transfer representations. The global mass balance of axial dispersed plug flow is described by the following (García-Mateos et al., 2015):

$$-D_L\frac{\partial^2 C}{\partial z^2}+\frac{\partial(vC)}{\partial z}+\frac{\partial C}{\partial t}+\left(\frac{1-\varepsilon}{\varepsilon}\right)\frac{\partial \overline{q}}{\partial t}=0 \tag{7}$$

where, ε is the porosity of column, v denotes the fluid superficial speed, C represents As(V) concentration (mg/L), and D_L stands for the axial dispersion coefficient (m^2/s).

The conditions of initial and boundary are (Lin et al., 2017; Sulaymon et al., 2009):

$$C = C_0,\ z = 0,\ t = 0 \tag{8}$$

$$C = 0,\ 0 < z \le L,\ t = 0 \tag{9}$$

$$D_L\frac{\partial C}{\partial z} = -v(C_0 - C),\ z = 0, t > 0 \tag{10}$$

$$\frac{\partial C}{\partial z} = 0, z = L, t \ge 0 \tag{11}$$

where L represents the column length (m).

According to Aguilera and Gutiérrez Ortiz (2016) and da Luz et al. (2018) the external film mass transfer coefficient (k_f) was estimated as follows:

$$k_f = \frac{D_m}{2R_p}(2.0 + 1.1\mathrm{Re}^{0.6}Sc^{0.33}) \tag{12}$$

$$\mathrm{Re} = \frac{2R_p v_s \rho_f}{\mu} \tag{13}$$

$$Sc = \frac{\mu}{D_m \rho_f} \tag{14}$$

where, Sc is the Schmidt number and Re is the Reynolds number. ρ_f, μ, and v_s represent density, viscosity, and fluid superficial velocity, respectively. D_m, or molecular diffusivity was estimated as follows (Miyabe and Isogai, 2011):

$$D_m = 7.4\times10^{-8}\frac{(\varnothing M_b)^{0.5}T}{\mu V_a^{0.6}} \tag{15}$$

where, V_a is the solute's molecular volume at its typical boiling temperature while T represents the temperature (K). Two parameters, $\varnothing$ and M, are the solvent and molecular weight-related parameters, respectively. V_a is computed as follows (Gomaa et al., 2017):

$$V_a = \frac{M}{\rho} - \frac{(\rho - \rho_0)}{m\rho\rho_0} \tag{16}$$

where, m is the solute's relative molar mass (kg/mol) and M is the solute molarity (mol/kg) of adsorbate. Meanwhile, ρ represents the solution's densities (g/cm^3) and ρ_0 stands for the densities (g/cm^3) of solvent.

3. Results and discussion

3.1. Batch adsorption studies

3.1.1. Equilibrium

Individual equilibrium adsorption experiments were conducted to assess the performance of the prepared Mn/Mg/Fe-LDH for adsorbing As (V) and As(III) ions. These experiments were carried out at 25 ± 1 °C and a constant pH of 7.0 ± 0.2 over a duration of 24 h. Although adsorption is a temperature-dependent process, this study focused on concentration-driven modeling under isothermal conditions. The model was designed to firstly validate concentration-dependent transport behavior, while future work will incorporate the temperature effects through thermodynamic parameter coupling. The Mn/Mg/Fe-LDH exhibits a heterogeneous surface (Section 3.2.1.2), making the Sips model suitable for analyzing its adsorption behavior. The Sips isotherm parameters calculated from As adsorption process by Mn/Mg/Fe-LDH are listed in Table 1, which including both process of As(V) and As(III). The results revealed that the Sips isotherm model exhibited an excellent fit to the experimental data, as evidenced by the high R^2 values (0.99) (Fig. 1). The respective maximum adsorption capacities of Mn/Mg/Fe-LDH for As(V) and As(III) were 42.88 and 66.55 mg/g. Notably, the adsorption capacity for As(III) was 35 % greater than that for As(V) when using Mn/Mg/Fe-LDH. This trend agrees with findings reported in previous research (Guo et al., 2007; Kim et al., 2012; Martinson and Reddy, 2009; Samsuri et al., 2013). However, a contrasting trend was observed by Choong et al. (2021) and Bagherifam et al. (2014) using Mg/Fe-LDH modified with polymers and SO_4^{2-}-intercalated Zn/Al-LDH in removing As(V) and As(III). Their findings indicated that these LDH-based materials demonstrated a higher adsorption capacity for As(V) compared to As(III). This discrepancy may be attributed to the different adsorption

Table 1
Sips isotherm constants of Mn/Mg/Fe-LDH for As(V) and As(III) adsorption.

Contaminant	Parameter	Unit	Value
As(V)	Q_m	mg/g	42.88
	b	L/mg	0.20
	n		1.92
	R^2		0.99
As(III)	Q_m	mg/g	66.55
	b	L/mg	0.12
	n		1.48
	R^2		0.99

mechanisms employed by LDH-based materials for removing As(V) and As(III). In this study, if anion exchange is the primary mechanism in the adsorption process, then Mn/Mg/Fe-LDH was expected to adsorb more As(V) anions than As(III) due to their exchange with host anions in the interlayer. However, the calculated maximum adsorption capacity (Q_m) for As(III) is greater than that for As(V). This suggests that other processes, particularly inner-sphere complexation, could significantly contribute to the uptake of As(III) by Mn/Mg/Fe-LDH, beyond the simple mechanism of anion exchange when part of As(III) is oxidized to As(V).

3.1.2. Adsorption kinetics

Single component kinetic adsorption experiments were undertaken at pH = 7.0 ± 0.2, and at 25 ± 1°C, with samples collected at various time intervals. The pore diffusion model (PDM) was applied to analyse the As(V) and As(III) kinetic adsorption. The Crank-Nicolson method was chosen to solve the differential equations associated with the PDM because it is stable and covers a broad spectrum of time and spatial discretization (Shirani et al., 2010).

The process of Mn/Mg/Fe-LDH adsorbing both As ions occurred within 2 h of the experiment's commencement (Fig. 2). The PDM adsorption parameters are summarized in Table 2. The obtained film mass transfer coefficients (k_f) for As(V) and As(III) were 4.00×10^{-4} and 5.00×10^{-4}, respectively. The values of D_p for both adsorbates were the same at 2.50×10^{-8}. As well, Fig. 2 illustrates the prediction curves under varying conditions, specifically different adsorbent doses vary from 0.50 to 1.00 g/L. Under these conditions the PDM successfully predicted the kinetic adsorption and as depicted in Fig. 2, the adsorption phenomenon can be estimated without conducting actual experiments. Unlike conventional empirical kinetic models (e.g., pseudo-first-order and pseudo-second-order), which are typically constrained to describing adsorption profiles over time under a single condition, the PDM enables broader prediction capabilities. Once parameters such as the film mass transfer coefficient (kf) and pore diffusion coefficient (Dp) are estimated from a base-case experimental dataset (e.g., at 0.5 g/L), they can be applied to simulate system performance under varying initial concentrations and flow rates. This transferability makes PDM particularly advantageous in modeling adsorption behavior without requiring extensive experimentation for every new scenario. These coefficients would be used for the simulation of adsorption in the column experiment (Section 3.2.3). The coefficient of determination (R^2) functioned as the primary metric for model fit assessment due to its clarity and widespread acceptance. The consistently high values obtained ($R^2 =$ 0.99) across conditions indicate excellent agreement between the experimental and modeled data, supporting the model's applicability. While additional error metrics (e.g., RMSE, χ^2) could offer further insight, the predictive performance demonstrated across multiple scenarios was deemed sufficient for this study.

3.2. Column adsorption studies

3.2.1. The properties of Mn/Mg/Fe-LDH

3.2.1.1. Crystal structure. After the column adsorption study, the structure's information of both pristine and As-laden Mn/Mg/Fe-LDH were examined using X-ray powder diffraction (XRD) techniques. As shown in Fig. 3, there is a visible change in the crystalline structure of As-laden Mn/Mg/Fe-LDH adsorbent after both As(III) and As(V) column adsorption processes differentiated to the pristine Mn/Mg/Fe-LDH. Remarkable changes were observed at 11.68°, 23.4°, and 29.4°. Firstly, the prominent diffraction peak observed at 29.4° was attributed to the forms of mineral nitrate ($NaNO_3$) in the pristine Mn/Mg/Fe-LDH, which was absent in the arsenic-laden Mn/Mg/Fe-LDH. This finding agrees with observations made in our previous study (Nguyen et al., 2022), where As-laden Mn/Mg/Fe-LDH was similarly analyzed after batch test. In the case of As(V)-laden Mn/Mg/Fe-LDH, the disappearance of the nitrate peak can be explained by the reaction between NO_3^- and As(V) anions via the anion exchange mechanism. Interestingly, the crystalline structure of As(III)-laden Mn/Mg/Fe-LDH closely resembles that of the As(V)-laden Mn/Mg/Fe-LDH. This means that As(III) oxidizes to As(V) before anion exchange between host anions NO_3^- and oxidized As(V) actually happens. Thus, the main mechanisms for removing As(III) using Mn/Mg/Fe-LDH were oxidation along with anion exchange, also known as oxidation coupled adsorption (Nguyen et al., 2022).

The presence of two peaks at 11.68° and 23.4° for the pristine adsorbent strongly suggests that Mn/Mg/Fe-LDH was successfully prepared using the process of co-precipitation from three commercial nitrate salts, namely Mn, Mg, and Fe (Pavlovic et al., 2016; Zhang et al., 2022). Yet, following the column adsorption the disappearance of these two diffraction peaks was recorded. This outcome indicates a significant alteration in the crystalline structure of Mn/Mg/Fe-LDH after the column adsorption process. This finding is consistent with results which were reported in earlier batch adsorption studies (Nguyen et al., 2022). The results noted the loss of the original crystalline structure in arsenic-laden Mn/Mg/Fe-LDH adsorbents. Fig. 3 also shows that the exchanged As anions in the adsorbent's interlayer space reacted with cations in the brucite-like layer (Fe), disfiguring the primeval structure of the adsorbent.

The remarkable similarity in the characterization of As-laden adsorbents after both column test and batch experiments suggests that the main mechanisms whereby Mn/Mg/Fe-LDH removed both As(V) and As(III) species were probably reduction-coupled adsorption and oxidation-coupled adsorption, respectively. Here, the reduction of As(V) to As(III)

Table 2
Kinetic parameters regarding As(V) and As(III) on Mn/Mg/Fe-LDH based on the PDM.

Adsorbate	Parameters	Value
As(V)	k_f, m/s	4.00×10^{-4}
	D_p, m^2/s^1	2.50×10^{-8}
	R^2	0.99
As(III)	k_f, m/s	5.00×10^{-4}
	D_p, m^2/s^1	2.50×10^{-8}
	R^2	0.99

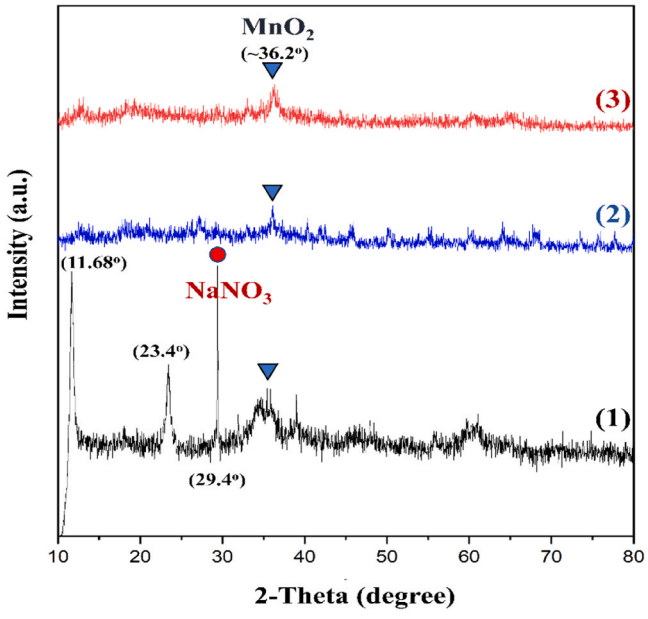

Fig. 3. XRD pattern of (1) pristine Mn/Mg/Fe-LDH, (2) As-laden Mn/Mg/Fe-LDH after As(III) column adsorption test, and (3) As-laden Mn/Mg/Fe-LDH after As(V) column adsorption test.

could have occurred. These findings, which align with our earlier research (Nguyen et al., 2022), highlight the complexity of the interactions between As species and the Mn/Mg/Fe-LDH structure. Consequently the dual roles of reduction and oxidation in enhancing adsorption efficiency are underscored. Moreover, a birnessite-type MnO_2 was found in both pristine Mn/Mg/Fe-LDH and As-laden Mn/Mg/Fe-LDH adsorbents (a peak at approximately 36.2°). The presence of MnO_2 in the LDH is also responsible for Mn/Mg/Fe-LDH removing As(V) and As(III) (Nguyen et al., 2022).

3.2.1.2. Surface functionality. FTIR analysis served to identify the primary functional groups that exist on the surfaces of both pristine and As-loaded Mn/Mg/Fe-LDH. Several significant bands on the adsorbent surface are illustrated in Fig. 4, including the band at around 3430 cm^{-1} (the OH groups), 594 cm^{-1} (the Fe–O groups), 420 cm^{-1} (the M–O and/or M–OH groups; where M presents Mg, Mn, and Fe). Notably, a well-identified band at about 1384 cm^{-1} has been credited to C═O overlapping with N = O, which is derived from CO_3^{2-} and NO_3^- ions, respectively. These functional groups are representative of the host anions found in the interlayer areas of the pristine Mn/Mg/Fe-LDH surface. Notably, this peak vanished from the surface of As-laden Mn/Mg/Fe-LDH once the column adsorption process was completed. Strongly indicated by this disappearance is that the anion exchange mechanism between As ions and anions in the adsorbent's interlayer regions is crucial for the effective uptake of As from aqueous environments by Mn/Mg/Fe-LDH. This finding for surface functional group of As-laden Mn/Mg/Fe-LDH after the column adsorption test is consistent with the batch experiment results concerning As-laden Mn/Mg/Fe-LDH (Nguyen et al., 2022).

3.2.1.3. Surface morphology. The morphology and main elemental components of both pristine and As-laden Mn/Mg/Fe-LDH were examined by SEM integrated with EDS (Fig. 5). As indicated in Fig. 5, the Mn/Mg/Fe-LDH adsorbents revealed a heterogeneous surface. As expected, the EDS analysis further confirmed the presence of essential elements (Mn, Mg, and Fe) on the pristine surface of Mn/Mg/Fe-LDH. This data is consistent with the XRD data, suggesting that Mn/Mg/Fe-LDH was successfully prepared from three commercial reagents via the co-precipitation method. Moreover, the EDS data of As-laden Mn/Mg/Fe-LDH adsorbents after As(III) and As(V) adsorption confirmed the presence of As, functioning as a significant component on As-laden Mn/Mg/Fe-LDH. This means that As(III) and As(V) ions were successfully taken up on the surface of Mn/Mg/Fe-LDH adsorbents.

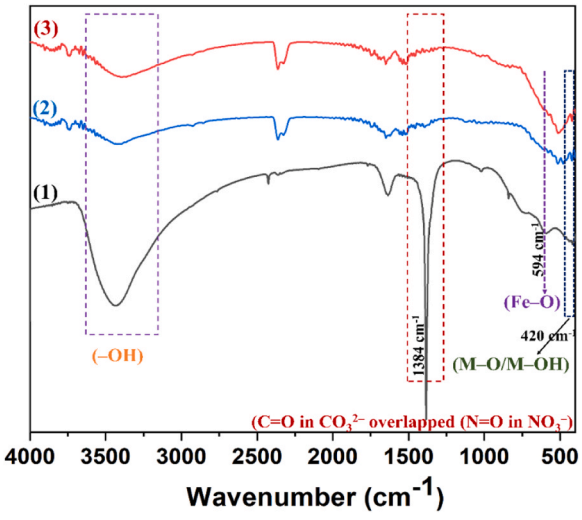

Fig. 4. FTIR spectrum of (1) pristine, (2) As-laden Mn/Mg/Fe-LDH after As(III) column adsorption test, and (3) As-laden Mn/Mg/Fe-LDH after As(V) column adsorption test.

3.2.2. Breakthrough curves

Mn/Mg/Fe-LDH's capacity to adsorb As ions from synthetic water was rigorously examined under continuous column conditions. The breakthrough curves for the adsorption process of As(V) and As(III) were plotted by measuring the output concentration ratio at a given time *t* (*Ct*) to the input concentration (*Co*) on the Y-axis versus time on the X-axis (Fig. 6). The modeling of breakthrough curves of the adsorption for As (V) and As(III) ions over 320 days were simulated successfully by the PDM incorporating the Sips equation (Fig. 6). The axial dispersion coefficient, D_L, was calculated as 2.00×10^{-6} for both breakthrough curves of As(V) and As(III) adsorption (Table 3). The As(V) breakthrough curves were steeper compared to those for As(III) ions. This indicates that As(V) underwent faster mass transfer and reached the saturation of the LDH adsorption sites more rapidly than As(III). This behavior could be attributed to the negatively charged As(V) species (e.g., $H_2AsO_4^-$, $HAsO_4^{2-}$), which exhibit stronger interactions with the LDH surface compared to the neutral As(III) species (Nguyen et al., 2020). Although the external film mass transfer coefficient for As(III) ($kf = 5.00 \times 10^{-4}$) is higher than that for As(V) ($kf = 4.00 \times 10^{-4}$) (Table 2), the neutral As(III) species in solution were oxidized to As(V) upon initial contact with the LDH material. Following this oxidation process, both the oxidized As(V) and the remaining As(III) were effectively removed from the solution via adsorption onto the LDH surface. Moreover, Nguyen et al. (2022) analyzed the adsorption kinetics of the LDH adsorbent for As(V) and As(III) using the pseudo-first-order and Elovich models. The results demonstrated that the initial adsorption rate constant for As(V) was nearly twice as high as that for As(III), indicating that the adsorption of As(V) began more rapidly. This contributed to a higher overall mass transfer rate for As(V) compared to As(III).

Obviously, the saturation time for Mn/Mg/Fe-LDH when adsorbing As(III) adsorbate was 280 days, which was longer than the 180 days for As(V). These results are consistent with the higher value of the Sips maximum adsorption capacity (Q_m) of Mn/Mg/Fe-LDH for As(III) obtained in the batch adsorption experiments. The Q_m of Mn/Mg/Fe-LDH toward As(III) was 66.55 mg/g, representing a 35 % increase compared to Q_m for As(V) (42.88 mg/g). The experimental data confirmed that the residual concentrations of As(V) and As(III) in the filtered water exceeded the WHO recommended limit for As in drinking water (0.01 mg/L) after 30 and 40 days, respectively. These results strongly suggest that, in field applications, filter replacement is necessary before these time points are reached to ensure As concentrations are within the permissible limits of water safety.

While the model captures the overall trend of breakthrough behavior, some deviations were observed between experimental and simulated results, particularly an earlier-than-predicted breakthrough inflection for As(III) (Fig. 6b). This discrepancy may be attributed to physical phenomena not fully captured by the model, such as minor packing inconsistencies, adsorbent aggregation, or flow channeling, which could reduce the effective contact time between the adsorbate and adsorbent. Additionally, the film mass transfer and pore diffusion coefficients used in the model were estimated from batch conditions and assumed to remain constant; however, these parameters may vary under long-term flow operation. Finally, the assumptions of ideal plug flow and uniform adsorbent properties may oversimplify the actual behavior in the fixed-bed column, especially over extended durations. Despite these limitations, the model: firstly, demonstrates strong predictive capability; and secondly, highlights the importance of validating dynamic models under realistic column conditions.

3.2.3. Model predictions of breakthrough curves

Simulating the breakthrough curves in the column adsorption study for both As(V) and As(III) was carried out under the following conditions - length of bed (0.045 – 0.135 m), superficial filtration rate (0.75–1.25 m/h), and initial concentration (0.033–3.333 mg/L) - to

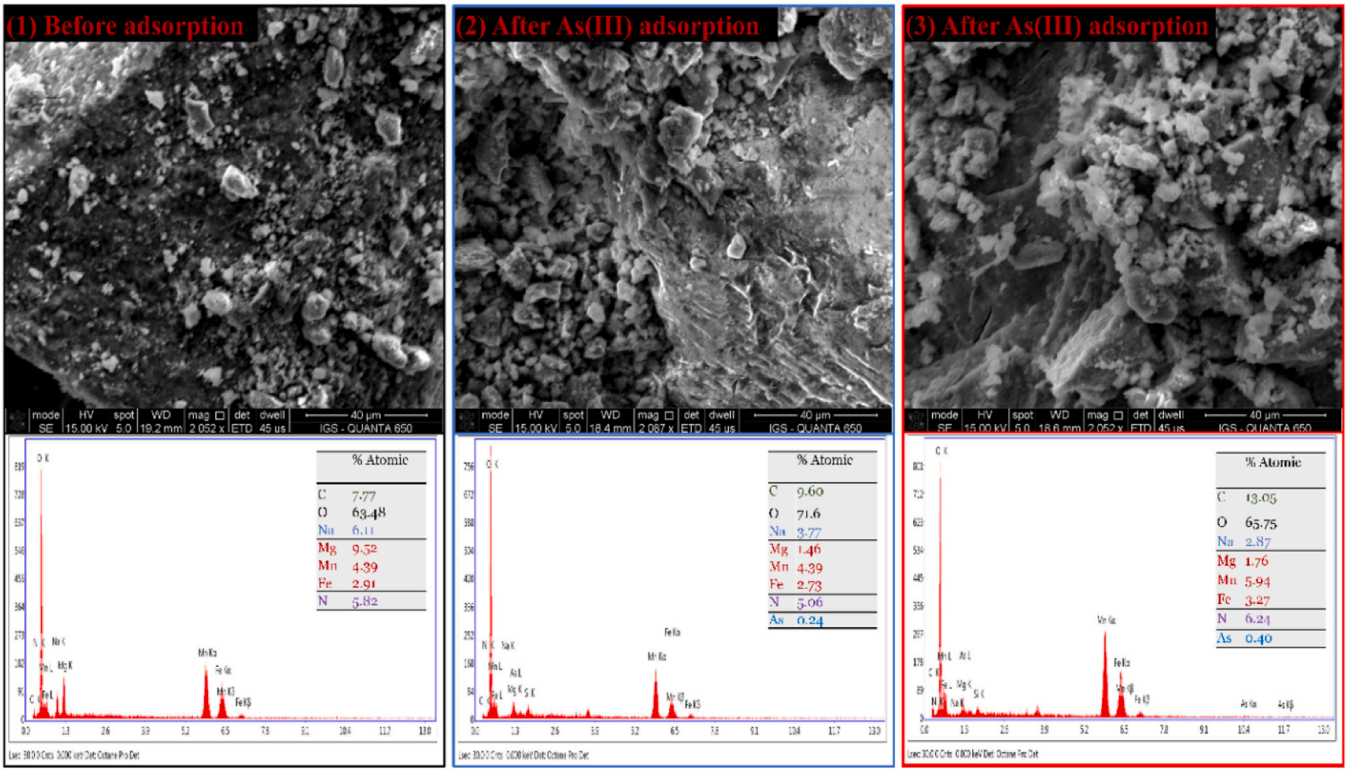

Fig. 5. SEM micrographs and EDS results of (1) pristine, (2) As-laden Mn/Mg/Fe-LDH after As(III) column adsorption test, and (3) As-laden Mn/Mg/Fe-LDH after As (V) column adsorption test.

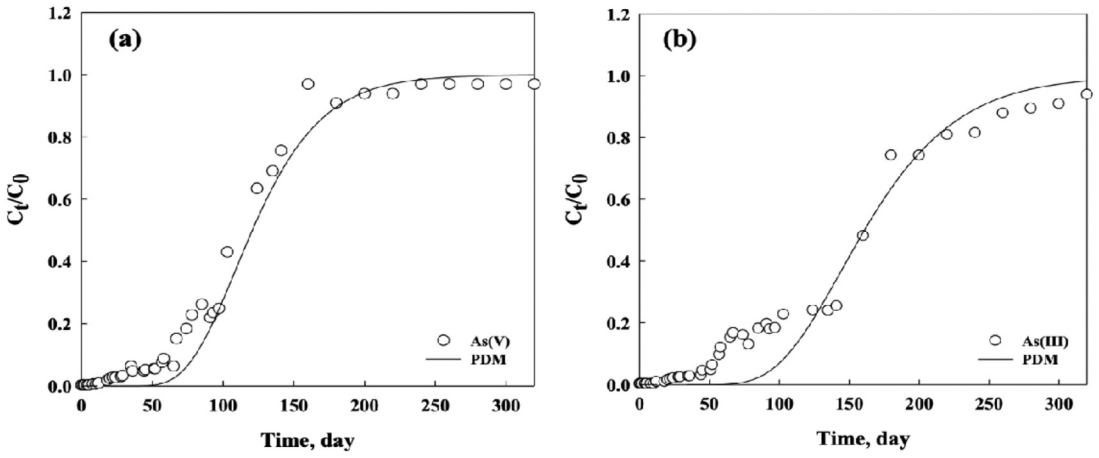

Fig. 6. Single component breakthrough prediction curves of (a) As(V) and (b) As(III) adsorption on Mn/Mg/Fe-LDH.

Table 3
Column adsorption parameters.

Adsorbate	Parameters	Unit	Value
As(V)	D_L	m^2/s	2.00×10^{-6}
As(III)	D_L	m^2/s	2.00×10^{-6}

assess the model's accuracy and overall performance. These factors were estimated through the mathematical column adsorption dynamic model incorporating the Sips isotherm parameters to demonstrate the adsorption behavior in the adsorbent's fixed bed adsorption column system (Naja and Volesky, 2006).

The curves in Fig. 7-(a) and (d) were simulated under conditions of 0.333 mg/L of feed concentration and 0.75 m/h of filtration rate and for varying column lengths. The data show that breakthrough times double and triple with an increase in the bed length which corresponds to the depth and amount of packed adsorbent. The superior adsorption efficiency and longer breakthrough time were obtained for 0.135 m bed length. This can be attributed to the adsorbent's increased specific surface area and a larger number of available binding sites at higher bed heights, which led to a corresponding increase in the total adsorbed As ions. Furthermore, as the bed depth increased, the mass transfer zone widened, resulting in moderately steeper breakthrough curves. With increased bed depth, diffusion mass transfer became the dominant mechanism, overshadowing the axial dispersion phenomenon. As a result, a significant increase in breakthrough time was observed. As reported by Riazi et al. (2016), higher bed heights in a fixed-bed column are beneficial for improving performance because they provide more

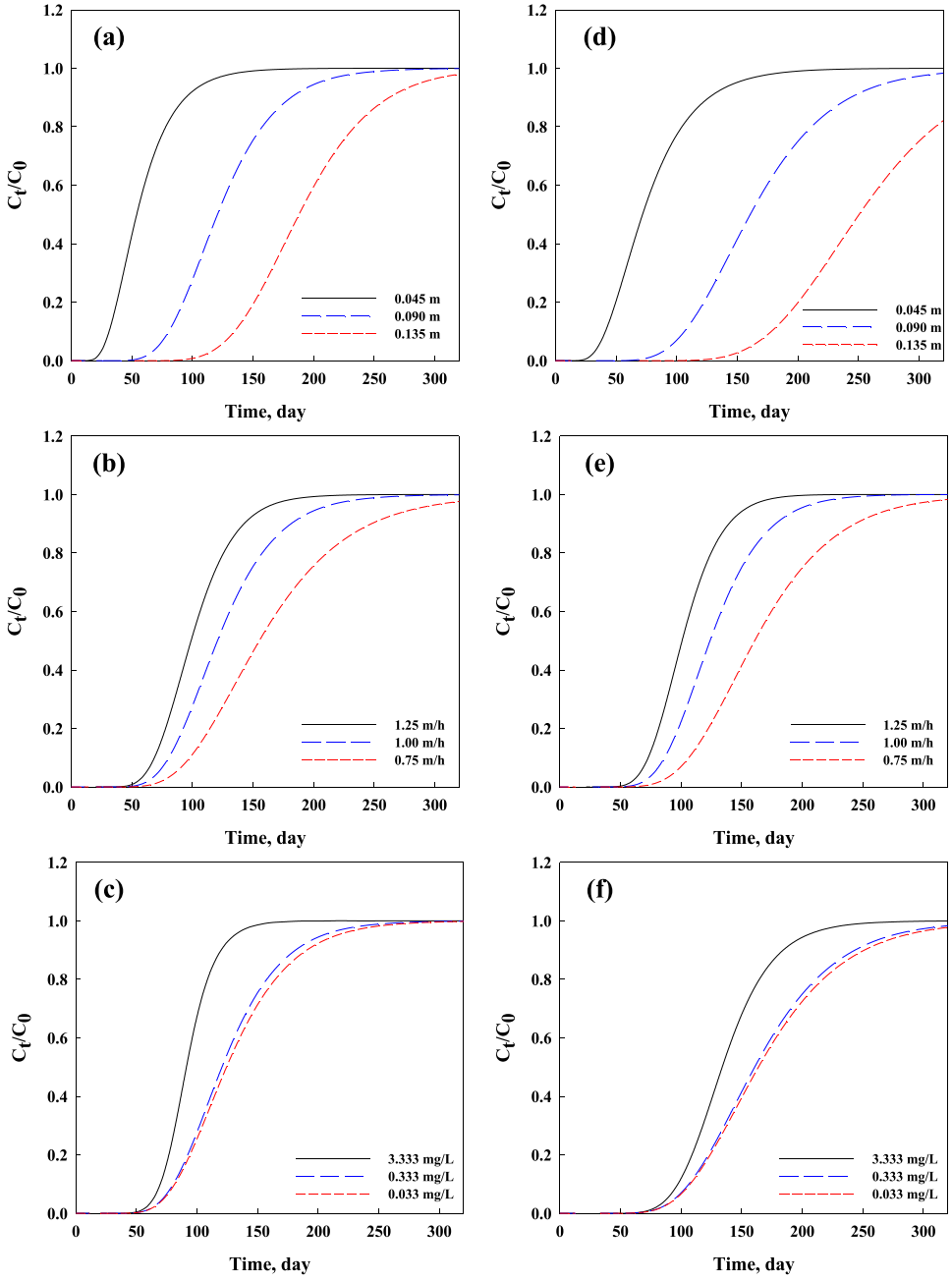

Fig. 7. Breakthrough curves simulation of single component for (a to c) As(V) and (d to f) As(III) in terms of length of bed (m), (b) filtration rate (m/h) and (c) initial feed concentration (mg/L).

active binding sites for metal ion adsorption.

The effect of the filtration rate is shown in Fig. 7-(b) and (e) for As(V) and As(III) column adsorption simulation results. These simulation conditions were for 0.09 m of column length and 0.333 mg/L of feed concentration. Rapid flow of the feed not only shortens the breakthrough time but also makes the breakthrough curves steeper. This implies that the concentration gradient is a major factor influencing the time of breakthrough and the saturation limit (García-Mateos et al., 2015).

The last two graphs (Fig. 7-(c) and (f)) illustrate the simulation results for varying feed concentrations at 0.09 m bed length and 0.75 m/h filtration rate. Interestingly, the breakthrough curves at 0.0333 and 0.333 mg/L inlet concentrations show relatively similar profiles despite the 10-fold increase in influent concentration. This can be explained by the low-concentration curvature of the Sips isotherm, where adsorption capacity increases sub-linearly due to limited site occupancy. The driving force for mass transfer remains low in this range, resulting in a relatively slow-moving mass transfer zone. In contrast, at 3.333 mg/L, the inlet concentration lies in the nonlinear regime of the isotherm, where the available adsorption sites are rapidly saturated, leading to a much faster breakthrough.

4. Conclusions

This study has used the pore diffusion model (PDM) incorporated with the Sips equation model, in an attempt to rate the ability of Mn/Mg/Fe-LDH to uptake As ions (As(III) and As(V)) from synthetic water in batch and fix-bed column experiments. Results from analyzing the adsorbent's characterization suggested that the oxidation - coupled adsorption and reduction-coupled oxidation were probably the primary

As(III) and As(V) ions adsorption mechanisms, respectively. Additionally, the results indicate that the equilibrium and kinetic processes of the Mn/Mg/Fe-LDH adsorption toward As(III) and As(V) were effectively fitted by the Sips equation and PDM model, respectively. The coefficients including pore diffusion (D_p) and mass transfer (k_f) derived from the PDM model were instrumental in simulating the column adsorption behavior. The experimental data calculated from the column adsorption test confirmed that the As(V) and As(III) breakthrough curves were satisfactorily represented by the PDM integrated with the Sips equation. Furthermore, the models that were deployed successfully predicted the breakthrough curves for a range of adsorption settings, for example bed height of 0.045–0.135 m, filtration rate of 0.75–1.25 m/h, and input As(V) concentration from 0.033 to 3.333 mg/L. These findings demonstrated that the modelling and simulating the breakthrough curves of adsorbents in removing As contaminants bring significant advantages and can be applied in the water treatment industry. The model could be able to predict the breakthrough curves in water filter systems which is essential for designing and operating filter systems efficiently. The ability to accurately simulate adsorption behavior under different operational conditions such as initial contaminant concentrations and flow rates will help engineers reduce extensive experimental requirements and costly trials. This will finally lead to improved operational efficiency and lower treatment costs.

CRediT authorship contribution statement

Tien Vinh Nguyen: Writing – review & editing, Supervision, Methodology, Conceptualization. **Thi Hai Nguyen:** Writing – original draft, Validation, Methodology, Investigation, Formal analysis. **Seongchul Ryu:** Writing – original draft, Investigation, Formal analysis. **Paripurnanda Loganathan:** Writing – review & editing, Methodology. **Jaya Kandasamy:** Writing – review & editing, Methodology. **Saravanamuthu Vigneswaran:** Writing – review & editing, Supervision, Methodology, Conceptualization.

Declaration of Competing Interest

The authors declare that they have no known competing financial interests or personal relationships that could have appeared to influence the work reported in this paper.

Acknowledgement

Nguyen Thi Hai was funded by the Postdoctoral Scholarship Programme of Vingroup Innovation Foundation (VINIF), code VINIF.2024.STS.23.

References

Aguilera, P.G., Gutiérrez Ortiz, F.J., 2016. Prediction of fixed-bed breakthrough curves for H2S adsorption from biogas: importance of axial dispersion for design. Chem. Eng. J. 289, 93–98. https://doi.org/10.1016/j.cej.2015.12.075.

Asiabi, H., Yamini, Y., Shamsayei, M., 2017. Highly selective and efficient removal of arsenic(V), chromium(VI) and selenium(VI) oxyanions by layered double hydroxide intercalated with zwitterionic glycine. J. Hazard. Mater. 339, 239–247. https://doi.org/10.1016/j.jhazmat.2017.06.042.

Bagherifam, S., Komarneni, S., Lakzian, A., Fotovat, A., Khorasani, R., Huang, W., Ma, J., Wang, Y., 2014. Evaluation of Zn–Al–SO4 layered double hydroxide for the removal of arsenite and arsenate from a simulated soil solution: isotherms and kinetics. Appl. Clay Sci. 95, 119–125. https://doi.org/10.1016/j.clay.2014.02.028.

Brion-Roby, R., Gagnon, J., Deschênes, J.-S., Chabot, B., 2018. Investigation of fixed bed adsorption column operation parameters using a chitosan material for treatment of arsenate contaminated water. J. Environ. Chem. Eng. 6, 505–511. https://doi.org/10.1016/j.jece.2017.12.032.

Choong, C.E., Wong, K.T., Jang, S.B., Saravanan, P., Park, C., Kim, S.-H., Jeon, B.-H., Choi, J., Yoon, Y., Jang, M., 2021. Granular Mg-Fe layered double hydroxide prepared using dual polymers: insights into synergistic removal of As(III) and As(V). J. Hazard. Mater. 403, 123883. https://doi.org/10.1016/j.jhazmat.2020.123883.

Chu, K.H., 2020. Breakthrough curve analysis by simplistic models of fixed bed adsorption: in defense of the century-old Bohart-Adams model. Chem. Eng. J. 380, 122513. https://doi.org/10.1016/j.cej.2019.122513.

Cruz-Olivares, J., Pérez-Alonso, C., Barrera-Díaz, C., Ureña-Nuñez, F., Chaparro-Mercado, M.C., Bilyeu, B., 2013. Modeling of lead (II) biosorption by residue of allspice in a fixed-bed column. Chem. Eng. J. 228, 21–27. https://doi.org/10.1016/j.cej.2013.04.101.

García-Mateos, F.J., Ruiz-Rosas, R., Marqués, M.D., Cotoruelo, L.M., Rodríguez-Mirasol, J., Cordero, T., 2015. Removal of paracetamol on biomass-derived activated carbon: modeling the fixed bed breakthrough curves using batch adsorption experiments. Chem. Eng. J. 279, 18–30. https://doi.org/10.1016/j.cej.2015.04.144.

Gomaa, E.A., Negm, A., Tahoon, M.A., 2017. Conductometric and volumetric study of copper sulphate in aqueous ethanol solutions at different temperatures. J. Taibah Univ. Sci. 11, 741–748. https://doi.org/10.1016/j.jtusci.2016.08.007.

Guo, H., Stüben, D., Berner, Z., 2007. Adsorption of arsenic(III) and arsenic(V) from groundwater using natural siderite as the adsorbent. J. Colloid Interface Sci. 315, 47–53. https://doi.org/10.1016/j.jcis.2007.06.035.

Inglezakis, V.J., Fyrillas, M.M., Stylianou, M.A., 2018. Two-phase homogeneous diffusion model for the fixed bed sorption of heavy metals on natural zeolites. Microporous Mesoporous Mater. 266, 164–176. https://doi.org/10.1016/j.micromeso.2018.02.045.

Jain, N., Chandramani, S., 2018. Arsenic poisoning- an overview. Indian J. Med. Spec. 9, 143–145. https://doi.org/10.1016/j.injms.2018.04.006.

Kalaruban, M., Loganathan, P., Nguyen, T.V., Nur, T., Hasan Johir, M.A., Nguyen, T.H., Trinh, M.V., Vigneswaran, S., 2019. Iron-impregnated granular activated carbon for arsenic removal: application to practical column filters. J. Environ. Manag. 239, 235–243. https://doi.org/10.1016/j.jenvman.2019.03.053.

Kim, J.Y., Balathanigaimani, M.S., Moon, H., 2015. Adsorptive removal of nitrate and phosphate using MCM-48, SBA-15, chitosan, and volcanic Pumice. Water Air Soil Poll. 226, 431. https://doi.org/10.1007/s11270-015-2692-z.

Kim, Y.-S., Kim, D.-H., Yang, J.-S., Baek, K., 2012. Adsorption characteristics of As(III) and As(V) on alum sludge from water purification facilities. Sep. Sci. Technol. 47, 2211–2217. ⟨https://www.tandfonline.com/doi/abs/10.1080/01496395.2012.700676⟩.

Lata, S., Samadder, S.R., 2016. Removal of arsenic from water using nano adsorbents and challenges: a review. J. Environ. Manag. 166, 387–406. https://doi.org/10.1016/j.jenvman.2015.10.039.

Lin, X., Huang, Q., Qi, G., Shi, S., Xiong, L., Huang, C., Chen, X., Li, H., Chen, X., 2017. Estimation of fixed-bed column parameters and mathematical modeling of breakthrough behaviors for adsorption of levulinic acid from aqueous solution using SY-01 resin. Sep. Purif. Technol. 174, 222–231. https://doi.org/10.1016/j.seppur.2016.10.016.

Lin, L., Qiu, W., Wang, D., Huang, Q., Song, Z., Chau, H.W., 2017. Arsenic removal in aqueous solution by a novel Fe-Mn modified biochar composite: characterization and mechanism. Ecotoxicol. Environ. Saf. 144, 514–521. https://doi.org/10.1016/j.ecoenv.2017.06.063.

Lu, H., Zhu, Z., Zhang, H., Zhu, J., Qiu, Y., 2015. Simultaneous removal of arsenate and antimonate in simulated and practical water samples by adsorption onto Zn/Fe layered double hydroxide. Chem. Eng. J. 276, 365–375. https://doi.org/10.1016/j.cej.2015.04.095.

Luengo, C.V., Lopez, N.A., Ramos, C.P., Avena, M.J., 2023. Highly efficient arsenic adsorption onto Mg/Al/Fe layered double hydroxides: Kinetics, isotherm, XPS and Mössbauer spectroscopies. J. Water Process Eng. 56, 104542. https://doi.org/10.1016/j.jwpe.2023.104542.

da Luz, C., de Arruda Guelli Ulson de Souza, S.M., Ulson de Souza, A.A., Dervanoski, A., de Oliveira Samel Moraes, A., Wood, B.D., 2018. A multiscale model for carbon adsorption of BTX compounds: comparison of volume averaging theory and experimental measurements. Chem. Eng. Sci. 184, 285–308. https://doi.org/10.1016/j.ces.2018.02.047.

Martinson, C.A., Reddy, K.J., 2009. Adsorption of arsenic(III) and arsenic(V) by cupric oxide nanoparticles. J. Colloid Interface Sci. 336, 406–411. https://doi.org/10.1016/j.jcis.2009.04.075.

Miyabe, K., Isogai, R., 2011. Estimation of molecular diffusivity in liquid phase systems by the Wilke–Chang equation. J. Chromatogr. A 1218, 6639–6645. https://doi.org/10.1016/j.chroma.2011.07.018.

Naja, G., Volesky, B., 2006. Behavior of the mass transfer zone in a biosorption column. Environ. Sci. Technol. 40, 3996–4003. https://doi.org/10.1021/es051542p.

Nguyen, T.T.Q., Loganathan, P., Nguyen, T.V., Vigneswaran, S., Ngo, H.H., 2020. Iron and zirconium modified luffa fibre as an effective bioadsorbent to remove arsenic from drinking water. Chemosphere 258, 127370. https://doi.org/10.1016/j.chemosphere.2020.127370.

Nguyen, T.H., Ryu, S., Loganathan, P., Kandasamy, J., Nguyen, T.V., Vigneswaran, S., 2022. Arsenic adsorption by low-cost laterite column: long-term experiments and dynamic column modeling. Process Saf. Environ. Prot. 160, 868–875. https://doi.org/10.1016/j.psep.2022.03.010.

Nguyen, T.H., Tran, H.N., Nguyen, T.V., Vigneswaran, S., Trinh, V.T., Nguyen, T.D., Ha Nguyen, T.H., Mai, T.N., Chao, H.-P., 2022. Single-step removal of arsenite ions from water through oxidation-coupled adsorption using Mn/Mg/Fe layered double hydroxide as catalyst and adsorbent. Chemosphere 295, 133370. https://doi.org/10.1016/j.chemosphere.2021.133370.

Nguyen, T.H., Tran, H.N., Vu, H.A., Trinh, M.V., Nguyen, T.V., Loganathan, P., Vigneswaran, S., Nguyen, T.M., Trinh, V.T., Vu, D.L., Nguyen, T.H.H., 2020. Laterite as a low-cost adsorbent in a sustainable decentralized filtration system to remove arsenic from groundwater in Vietnam. Sci. Total Environ. 699, 134267. https://doi.org/10.1016/j.scitotenv.2019.134267.

Pavlovic, M., Huber, R., Adok-Sipiczki, M., Nardin, C., Szilagyi, I., 2016. Ion specific effects on the stability of layered double hydroxide colloids. Soft Matter 12, 4024–4033. https://doi.org/10.1039/C5SM03023D.

Pena, M.E., Korfiatis, G.P., Patel, M., Lippincott, L., Meng, X., 2005. Adsorption of As(V) and As(III) by nanocrystalline titanium dioxide. Water Res. 39, 2327–2337. https://doi.org/10.1016/j.watres.2005.04.006.

Ponnusami, V., Rajan, K.S., Srivastava, S.N., 2010. Application of film-pore diffusion model for methylene blue adsorption onto plant leaf powders. Chem. Eng. J. 163, 236–242. https://doi.org/10.1016/j.cej.2010.07.052.

Riazi, M., Keshtkar, A.R., Moosavian, M.A., 2016. Biosorption of Th(IV) in a fixed-bed column by Ca-pretreated Cystoseira indica. J. Environ. Chem. Eng. 4, 1890–1898. https://doi.org/10.1016/j.jece.2016.03.017.

Samsuri, A.W., Sadegh-Zadeh, F., Seh-Bardan, B.J., 2013. Adsorption of As(III) and As(V) by Fe coated biochars and biochars produced from empty fruit bunch and rice husk. J. Environ. Chem. Eng. 1, 981–988. https://doi.org/10.1016/j.jece.2013.08.009.

Shirani, B., Kaghazchi, T., Beheshti, M., 2010. Water and mercaptan adsorption on 13X zeolite in natural gas purification process. Korean J. Chem. Eng. 27, 253–260. https://doi.org/10.1007/s11814-009-0327-z.

Siddiqui, S.I., Chaudhry, S.A., 2017. Iron oxide and its modified forms as an adsorbent for arsenic removal: a comprehensive recent advancement. Process Saf. Environ. Prot. 111, 592–626. https://doi.org/10.1016/j.psep.2017.08.009.

Singh, P., Borthakur, A., Singh, R., Bhadouria, R., Singh, V.K., Devi, P., 2021. A critical review on the research trends and emerging technologies for arsenic decontamination from water. Groundw. Sustain. Dev. 14, 100607. https://doi.org/10.1016/j.gsd.2021.100607.

Smedley, P.L., Kinniburgh, D.G., 2002. A review of the source, behaviour and distribution of arsenic in natural waters. Appl. Geochem. 17, 517–568. https://doi.org/10.1016/S0883-2927(02)00018-5.

Sulaymon, A.H., Abid, B.A., Al-Najar, J.A., 2009. Removal of lead copper chromium and cobalt ions onto granular activated carbon in batch and fixed-bed adsorbers. Chem. Eng. J. 155, 647–653. https://doi.org/10.1016/j.cej.2009.08.021.

Tran, H.N., Nguyen, D.T., Le, G.T., Tomul, F., Lima, E.C., Woo, S.H., Sarmah, A.K., Nguyen, H.Q., Nguyen, P.T., Nguyen, D.D., Nguyen, T.V., Vigneswaran, S., Vo, D.-V. N., Chao, H.-P., 2019. Adsorption mechanism of hexavalent chromium onto layered double hydroxides-based adsorbents: a systematic in-depth review. J. Hazard. Mater. 373, 258–270. https://doi.org/10.1016/j.jhazmat.2019.03.018.

Vancea, C., Mladin, G., Ciopec, M., Negrea, A., Duteanu, N., Negrea, P., Mosoarca, G., Ianasi, C., 2023. Arsenic removal using unconventional material with iron content: batch adsorption and column study. Toxics 11. ⟨https://www.mdpi.com/2305-6304/11/10/849⟩.

Wang, J., Zhang, T., Li, M., Yang, Y., Lu, P., Ning, P., Wang, Q., 2018. Arsenic removal from water/wastewater using layered double hydroxide derived adsorbents, a critical review. RSC Adv. 8, 22694–22709. https://doi.org/10.1039/C8RA03647K.

Weerasundara, L., Ok, Y.-S., Bundschuh, J., 2021. Selective removal of arsenic in water: a critical review. Environ. Pollut. 268, 115668. https://doi.org/10.1016/j.envpol.2020.115668.

Zhang, Y., Cao, J., Li, J., Yuan, Z., Li, D., Wang, L., Han, W., 2022. Self-assembled Cobalt-doped NiMn-layered double hydroxide (LDH)/V2CTx MXene hybrids for advanced aqueous electrochemical energy storage properties. Chem. Eng. J. 430, 132992. https://doi.org/10.1016/j.cej.2021.132992.